

Review

Electron Transfer through Molecules and Assemblies at Electrode Surfaces

Burak Ulgut, and Hector D. Abruna

Chem. Rev., **2008**, 108 (7), 2721-2736 • DOI: 10.1021/cr068060w • Publication Date (Web): 11 July 2008

Downloaded from <http://pubs.acs.org> on December 24, 2008

More About This Article

Additional resources and features associated with this article are available within the HTML version:

- Supporting Information
- Links to the 1 articles that cite this article, as of the time of this article download
- Access to high resolution figures
- Links to articles and content related to this article
- Copyright permission to reproduce figures and/or text from this article

[View the Full Text HTML](#)

Electron Transfer through Molecules and Assemblies at Electrode Surfaces

Burak Ulgut and Héctor D. Abruña*

Department of Chemistry and Chemical Biology, Baker Laboratory, Cornell University, Ithaca, New York 14853-1301

Received October 23, 2007

Contents

1. Introduction	2721
2. Theoretical Models	2722
3. Monolayer Experiments	2724
3.1. Break Junctions	2724
3.1.1. Triple Beam Mechanical Break Junctions	2724
3.1.2. Break Junctions Based on STM	2726
3.1.3. Electromigrated Break Junctions	2728
3.2. Sandwich Junctions	2730
3.2.1. Evaporation of Metals	2730
3.2.2. Electroless Deposition Followed by Electrodeposition	2731
3.2.3. A Liquid Metal Brought into Contact	2732
3.2.4. Mechanical Contact Electrodes	2733
3.3. Scanning Tunneling Microscopy	2734
4. Conclusions	2735
5. Acknowledgments	2735
6. References	2735

1. Introduction

Chemically modified electrodes were first introduced to the scope of electrochemistry by Anson, Bard, Murray, Savéant, and others about three decades ago in an effort to provide selectivity to highly sensitive electrode surfaces.¹ While electrochemical techniques had high sensitivity because of the availability of accurate current measurement techniques, the lack of any differential selectivity of electrodes for analytes over impurities complicated the analysis. A functionalized electrode however would and does give the opportunity to chemically modify the surface of an electrode, providing the means to make the surface much more chemically selective.

In addition to the numerous contributions to the field of electrochemical biosensors² (for example, in the field of electrochemical biosensing, the lock and key enzyme substrate relationship can be exploited by immobilizing an enzyme on the electrode surface to analyze a solution of the substrate even in the presence of impurities; major contributions in this field are presented in a recent review by Bakker and Qin²), chemically modified electrodes opened up the possibility for electrochemists to be able to investigate electron transfer on electrode surfaces while side-stepping most of the mass transport problems (note that counterion diffusion and solvent rearrangement still have to take place). Once reliable techniques for modifying electrode surfaces were established, molecules with well positioned redox centers and with tunable redox potentials could be placed

on electrode surfaces to be able to systematically vary and observe the effects of important parameters such as distance,³ and chemical environment,⁴ among others. For example, the work by Chidsey et. al⁵ describes long-range electron transfer making use of exquisite control over the placement of the redox active site relative to the electrode surface. In more recent work, Amatore et. al⁴ investigated the effects of chemical environment on electron transfer by making mixed monolayers of electroinactive alkanes with compounds with well-defined redox centers.

Molecular electronics can also be dated to similar times as chemically modified electrodes. Though it has been argued that molecular electronics dates back to the days of Mulliken and his proposals of charge transfer salts,⁶ the general consensus is that the popularization of the field dates back to the cornerstone paper by Aviram and Ratner in 1974⁷ in which they proposed a molecular structure that should act as a diode when electron transport was measured across it. They designed the molecule based on a donor-bridge-acceptor model and calculated the electron transport with a semi empirical INDO approach. A number of experimental methods have been proposed to measure conductance through molecules and molecular assemblies since then including scanned probe techniques, mercury drop electrodes, electrical or mechanical break junctions, sandwich electrodes, and others. The common concept in all of these methods is to be able to “wire” the molecules between two electrodes (generally metallic, though semiconductors are also employed in some rare cases) and measure current as a function of an applied potential. A third electrode (gate) coupled through an electronically insulating dielectric is generally used to modulate the electrostatics around the active material, changing, in a deliberate fashion, its electronic energy levels. If the device is immersed in an electrolyte solution, the gate electrode takes on the role of the more traditional reference electrode with identical function.

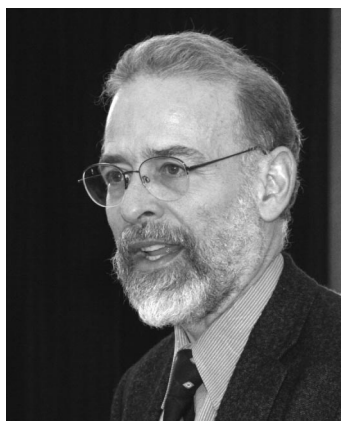
In nearly all efforts related to measuring conductance across molecules and molecular assemblies, the experiments have been based on making a chemically modified electrode to establish the first electrode–molecule contact. The second electrode is then either brought into contact temporarily (scanned probe) or permanently (crossbar, sandwich) or the single electrode is broken into two (break junctions) to measure those molecules that are statistically trapped across the junction. The over three decades experience in modifying electrodes’ electronic and physical properties puts electrochemistry at center stage for the molecular electronics efforts along with nanofabrication.

The experimental efforts on molecular electronics were pushed forward by two separate events. First, the development of scanning tunneling microscopy (STM) by Binnig and Rohrer in 1981, and second, the ever shrinking micro-

* To whom correspondence should be addressed. E-mail: hda1@cornell.edu.



Burak Ulgut received a B.S. in Chemistry from Bilkent University, Ankara, Turkey. He then joined Department of Chemistry at Cornell University and earned his Ph.D. in July 2007 under Prof. Héctor Abruña's supervision. He is currently a postdoctoral research associate under Prof. Sir R. Friend at the Cavendish Laboratory in Cambridge University. Dr. Ulgut is an enthusiastic soccer player and a Turkish folk dancer in his spare time.



Héctor D. Abruña received B.S. and M.S. degrees in Chemistry from Rensselaer Polytechnic Institute in 1975 and 1976, respectively. He received a Ph.D. in Chemistry from the University of North Carolina in Chapel Hill in 1980 under the direction of R. W. Murray and T. J. Meyer. He was a postdoctoral associate under A. J. Bard at the University of Texas at Austin from 1980 to 1981. He began his academic career as an Assistant Professor in the Chemistry Department at the University of Puerto Rico in 1982. In 1983 he moved to Cornell University, where he is currently the Émile M. Chamot Professor and Chair of the Department of Chemistry and Chemical Biology. He is most proud of the 32 students that, to date, have earned Ph.D. degrees under his supervision. Prof. Abruña is an avid runner, prodigious consumer of espresso, and in his spare time, and when the budget allows him to, he collects art from his native Puerto Rico with an emphasis on wooden sculptures.

electronic fabrication techniques approaching the dimensions of single molecules. Both developments made it possible to controllably and reversibly contact single molecules. In STM, because of the exponential decay of the tunneling current with tunneling distance, the current only involves those atoms that are on the very end (apex) of the microscope's tip. Depending on how sharp the tip is, there are only a small number of atoms (ideally a single atom) at the very end, making one of the contacts a single atom. Microfabrication techniques, on the other hand, have reached nanometer resolution with developments in e-beam lithography. Metallic electrodes with nanometer (and even subnanometer) spacing can be fabricated using a very tightly focused electron beam (~ 1 nm spot size) and appropriately designed resist materials.

On the theoretical side, the well-established theory of electron transfer of Marcus⁸ has been applied to electron

transfer between and within molecules. In a 1997⁹ review by Marcus, he discussed a number of areas to which his theory has been applied. These include photosynthesis, organic reactions, and donor acceptor complexes, among others. Despite all the success on molecular charge transfer, the usual form of Marcus theory is not applicable to the electron transfer between electrodes and molecules because of the continuum of states involved in the electrodes. New theories of electron transfer, using the nonequilibrium Green's functions formalism (NEGF), have been developed by Ratner, Nitzan, Hush, Datta, Guo, and Mujica¹⁰ and they have been able to successfully reproduce a number of different experimental findings.

In this paper, we will review some of the transport measurements that have been carried out with experimental schemes based on chemically or physically modified electrodes and some of the theoretical models used to understand them. However, in the interest of keeping this review manageable in size, it will not be exhaustive, given the vast amount of literature on the topic. We will only be able to cover some of the major contributions with the most general applicability. We will first briefly review the theoretical models outlining the major assumptions and the achievements of each one. We will then review different electrode geometries and fabrication methods to make metal–molecule–metal junctions and the resulting experimental findings. Finally, we will discuss relevant scanned probe techniques and their application to electron transport through assemblies on electrodes.

There are a number of excellent previous review papers in the literature including the reports by McCreery,¹¹ James et al.,¹² Chen et al.,¹³ and Nitzan et al.¹⁴

2. Theoretical Models

The first theory of conduction for atomic scale systems was proposed by Landauer¹⁵ in 1957. Assuming that elastic scattering dominates conduction, the scattering equations are solved to get the conductance. The theory predicts the total conductance as integral multiples of the quantum of conductance ($g_0 = 2e^2/h = (12.9 \text{ k}\Omega)^{-1}$). The number of (parallel) channels between the two electrodes (traverse) that the electron can move on determines how many quanta of conductance will be observed. The experimental test of this theory came out of a number of experiments with metal chains¹⁶ where the width (number of atoms) of the metal chain at the thinnest point determined the number of quanta as seen in Figure 1.

Even though the Landauer theory explains experimental results of conduction through a chain of metal atoms very well, it fails to explain conduction through molecules because it neglects two distinct properties: (1) the inelastic scattering and (2) the coupling of the contacts to the molecules. The first improvement over the Landauer theory was to include the coupling of electronic and nuclear motions to electron transfer rates as in the Marcus–Hush–Jortner formulation.¹⁷ (This formulation is an extension of the Marcus theory to include the higher frequency vibrational modes of the molecules involved, in addition to the phonon modes accounted for by the Marcus approach. The formulation was developed to explain photosynthetic phenomena.) The next improvement was to include the electrodes and the coupling of molecules to them. Early attempts at this problem were to include a small cluster of metal atoms bound to the molecules and to solve for the electronic structure accord-

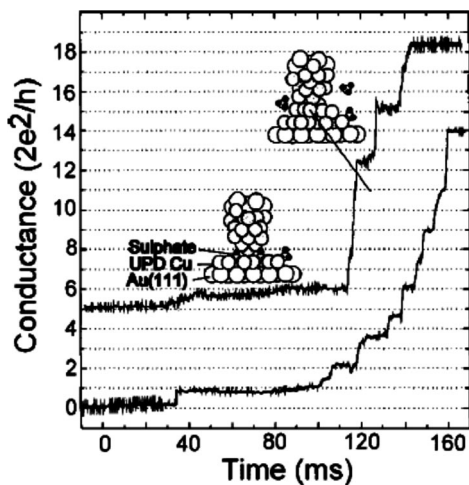


Figure 1. An electrochemical metal deposition carried across two closely spaced electrodes. The conductance of the electrochemically deposited metallic wire, as it grows, is plotted as a function of the growth time. Properly adjusting the growth conditions and following the conductance across the wire during the growth, discrete conductance steps of $2e^2/h$ (quantum of conductance) can be observed as the wire gets increasingly wider. The number of metal atoms at the thinnest point of the wire limits the conductance to a small number of conductance quanta (Reprinted with permission from ref 16. Copyright 1998 American Institute of Physics).

ingly.¹⁸ Even though the models were successful at predicting the geometry of the binding site, they were not useful for predicting conduction because they do not capture the continuum of electronic states in the metal. Using the NEGF formulation of transport theory,¹⁰ one can incorporate the coupling between the continuum of states in the metal and the discrete electronic states in the molecule. The calculations using the NEGF formulation and density functional theory (DFT) methodology have resulted in effective potential energy surfaces that lead to a qualitative agreement with the conductivity data taken for benzenedithiol molecules^{14,19} (Figure 2). The molecular vibrations can also be incorporated in the NEGF-DFT calculations to predict the inelastic electron tunneling spectroscopy (IETS)^{19–21} characteristics. The theory matches experiments very well for oligophenyleneethynylene (OPE), oligophenylenevinylene (OPV), and hexanedithiol (HDT) measured by Kushmerick et al.²² However, the theory does not capture any features arising from the $-S-Au$ bond, and the authors attribute the unexplained features to the metal molecule coupled vibrations.

A particularly important result using the NEGF method emphasizes the importance of the specifics of the contact between the molecule and gold electrodes.²³ Given the vastness of the structures that can arise during the formation of the break junctions, it is crucial to assess how much the electronic structure and conductivity are sensitive to the specifics of the geometry. Within the framework of the NEGF method, the transmission is shown to be a very strong function of the exact geometry over certain relevant length scales.

There have been a number of recent developments to the NEGF work explained above. A very significant development was reported by Sai et al.²⁴ in 2005. Using “time-dependent current-density functional theory” the correction to the static DFT calculations was analytically calculated and shown to increase the overall resistance for molecular junctions. Another improvement was reported by Toher et al.²⁵ also in 2005. This report involved an improvement over the ex-

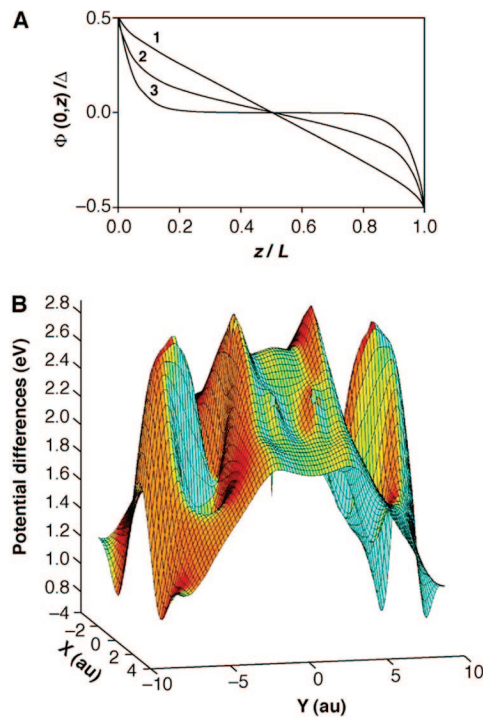


Figure 2. Potential energy calculations employing the DFT methodology. (A) The electrical potential plotted as a function of distance between two electrodes. The molecule in the middle was assumed to be a homogeneous cylinder (1,2,3 represent cylinder of increasing radii). Notice that with increasing diameter, the potential drop gets concentrated more toward the contacts. (B) The two-dimensional surface representing the potential drop plotted as a function of potential using a cylindrical model for the electrodes and a full benzene molecule in the middle. Notice the largest drop occurring on the actual atoms of the benzene molecule (Reprinted with permission from *Science* (<http://www.aaas.org>), ref 14. Copyright 2003 American Association for the Advancement of Science).

change correlation that was used in the previous reports, whereby the lack of derivative discontinuity that was inherent in the continuous local density approximation was removed by the implementation of an “atomic self-interaction correlation” that also resulted in an increase in the calculated overall resistance. The lack of derivative discontinuity in the electron density approximations (and the underestimation of the resistance thus resulting) were also addressed more recently by Koentopp et al.²⁶ The study yielded a new approach to calculate the exchange correlation corrections that have also shown that the previous standard NEGF studies overestimate the conductance.

The other model that has been very widely used is the one developed by Simmons in 1963.²⁷ The main reason that this model is employed is its simplicity, providing a convenient scale to compare different molecules. Current through an arbitrarily shaped potential barrier is exponentially dependent on the distance across the barrier and is given as $J = J_0 e^{-\beta d}$, where J_0 is the portion of the current defined at the minimum distance (i.e., contact resistance), d is the distance across the barrier, and β is a molecule-dependent parameter that defines how quickly the current density decays (for a detailed explanation of β and implications see Monnell et al.²⁸). β can be experimentally measured using a number of molecules of the same class, plotting the current density as a function of distance on a logarithmic plot and determining the slope. We will later refer to specific values of β and how they are measured.

An alternative method to the NEGF approaches was developed recently by Ortiz et al.²⁹ The method is based on the uncertainty relation ($\Delta E \delta t \geq \hbar/2$ combined with $I = \Delta Q / \Delta t$):

$$I \leq \frac{2\Delta Q \Delta E}{\hbar} \quad (1)$$

where ΔE is given as the potential difference across the system, and ΔQ is defined as the charge difference between the potential applied and free of potential on a chosen slab of the system using standard DFT codes. The currents calculated are of the same order of magnitude of the measured values. Different geometries have yielded qualitatively and quantitatively different I – V curves. Moreover, in certain geometries, the method yields nonmonotonous curves that exhibit peaks and negative differential resistance (NDR) which have been reportedly measured in some systems.

Finally, we would like to briefly mention the connection between the electron transfer rates used extensively to understand redox events and intramolecular charge transfer events to molecular conduction. The two events are intuitively similar given that in both systems electrons are flowing through molecules. The major difference, however, arises due to the continuum of states in a metal contact vs discrete levels in molecular electron transfer, and the energy dissipation mechanism being an electronic bath in the metal contacts vs a vibronic bath in the molecules. An excellent review on the similarities and differences of various theoretical aspects can be found in a chapter in the *Introduction to Molecular Electronics*.³⁰ For a donor–bridge–acceptor (DBA) system placed between two metallic electrodes, a linear expression can be shown³¹ within some assumptions:

$$g \approx \frac{8e^2}{\pi^2 \Gamma_D^{(L)} \Gamma_A^{(R)} F} k_{D \rightarrow A} \quad (2)$$

where g is the conductance, $\Gamma_D^{(L)}$ and $\Gamma_A^{(R)}$ are widths of D and A levels due to their couplings to the left and right metal leads, F is the Franck–Condon weighted density of states, and $k_{D \rightarrow A}$ is the rate of electron transfer from the donor to the acceptor. The weakest assumption on the proof is that the electronic structure of the molecular DBA complex is assumed to be the same in solution and between the electrodes. Though this assumption certainly will fail for nearly all experimental setups, it is still a good starting point since it captures the intuitive linear relationship.

3. Monolayer Experiments

A number of experiments attempting to measure conductance across single molecules make use of monolayers to achieve the decrease in dimensionality. Making and using a monolayer fixes one dimension to a single molecule thickness, allowing the use of already known techniques to achieve single molecule measurements. Break junctions, scanning tunneling microscopy, sandwich electrodes, and shadow evaporation are the four major methods that will be reviewed in what follows.

3.1. Break Junctions

In order to carry out electron transport measurements on single molecules, one needs to be able to interface macroscopic electronic measurement circuitry, that is, to “wire up”

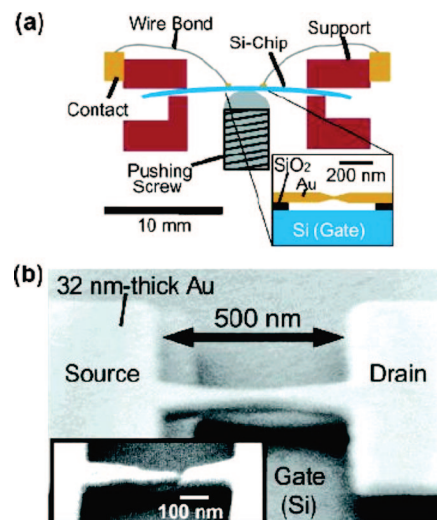


Figure 3. A triple beam mechanical break junction setup with gate electrode. (a) Schematic depicting the triple beam bending mechanism: the two red support pieces hold the two ends of the sample (Si-chip) and the pushing screw lifts the middle part. In this way, the sample is bent allowing for control of the gap across the electrodes. (b) An SEM of the active part of the device before breaking the gold bridge. The image was acquired with some tilt angle to make the space between the gold bridge and the gate visible. (Inset) The device after electromigration. (Reprinted with permission from ref 39. Copyright 2005 American Chemical Society).

individual molecules on two ends. Because conventional lithography is still short of delivering resolution at the molecular scale, break junctions, formed using several methods, have been employed.

Broadly, break junctions are formed by breaking a single metal wire into two sections leaving a gap between them. Three common methods to make junctions of this type are (1) mechanically through a triple beam bending mechanism, (2) mechanically through an STM based pulling mechanism, and (3) electromigration. None of them, however, allows for any control over the exact shape of the electrodes and thus contact to the molecule under investigation.

They do, however, provide some control on the width of the gap. With all the techniques, gaps in the sub nanometer range can routinely be achieved, allowing single molecule measurements to be done.

3.1.1. Triple Beam Mechanical Break Junctions

Triple beam mechanical break junctions (MBJs) were first established in 1985³² in an attempt to make Josephson Junctions (i.e., superconductor–insulator–superconductor), where appropriately chosen metals would act as the superconductors and vacuum would be the insulator. With a triple point bending mechanism (Figure 3) the strain on a glass slide (or silicon chip) is transferred, in turn, to the metallic electrode on the slide causing a break in the electrode. The metal vacuum metal junction is what is studied afterward with controlled electrode spacing to control the width of the insulating layer.

The first example of MBJs to make molecular junctions was by Reed et al. 1997.³³ The experimental procedure can be described as follows: a gold wire was covered with a self-assembled monolayer of 1,4-benzenedithiol, an organic molecule that can bind to two gold electrodes through the two thiol groups. The gold wire was subsequently stretched

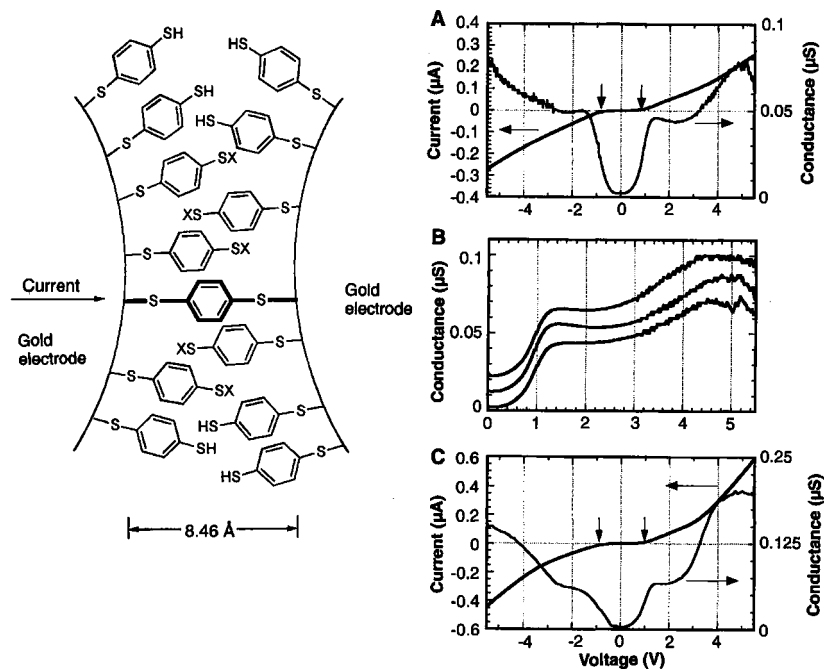


Figure 4. The assumed configuration and the I–V curves of the break junction experiment. (Left) The assumed configuration when the measurements are made. The benzenedithiol monolayer on the electrode is assumed to get trapped between the electrodes as the breaking proceeds. (Right) I–V curves taken. A and C represent two different configurations where two different conductance levels were observed with the configuration in C having twice the conductance of that of A. Graph B represents three independent measurement to show reproducibility, where the offset is added for clarity. (Reprinted with permission from *Science* (<http://www.aas.org>), ref 33. Copyright 1997 American Association for the Advancement of Science).

until breakage while in the assembly solution. Once the wire was broken, the solvent was evaporated and the wires were brought together until the “onset of conductance”. With the proper negative control experiments (performed the same way except without the molecules), the observed conductance could be ascribed to a small number (ideally one) of benzenedithiol molecules bridging the gap. Once the junction was established, current voltage curves were obtained as shown in Figure 4.

As seen in the figure, the data exhibit a conductance gap of ~ 2 V centered around zero bias, and conductance values of ~ 0.05 μS at higher biases in either direction. The I–V curves are symmetric consistent with the fact that the molecule is also symmetric.

This work led to an explosion of experimental as well as theoretical work, in addition to subsequent controversy. The major concern centered on the stability of a gold junction under a 5 V bias across 8 Å. With such a high electric field, and the known room temperature mobility of the gold atoms,³⁴ it is difficult to achieve a stable junction. Nevertheless, the paper was cited over 1300 times, and there has been an enormous amount of theoretical work attempting to model the observed conductance traces. Decent agreement has only recently been achieved, using the NEGF-DFT formalism explained above.³⁵

Using the same geometry, Reichert et al.³⁶ measured the conduction of different molecules both at room temperature and 30 K. They observed that the conductance curves reflected the symmetry, or asymmetry of the molecules. Employing modified triphenylene-ethylenes, they used two different molecules as shown in Figure 5. The anthracene derivative (i.e., symmetric) had peaks in conductance that were symmetrically placed with respect to zero bias, whereas the nitro derivative (i.e., asymmetric) only exhibited peaks of different intensity in forward and reverse bias. One general

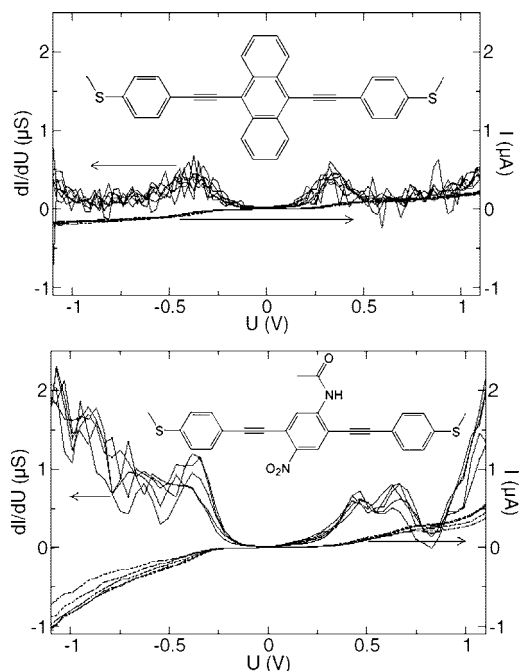


Figure 5. Two different molecules measured using a two-electrode mechanical break junction. The conductance of a symmetric (top) and an asymmetric (bottom) oligophenyleneethynylene derivative measured using the same setup. Multiple measurements are presented to show the variation of the curves. Notice the apparent symmetry (or lack thereof) of the molecules being reflected in the conductance curves as symmetric (or not) about zero voltage. (Reprinted with permission from ref 36. Copyright 2002 by the American Physical Society).

assumption in these experiments is that the two contacts are chemically and electrostatically equivalent. However, in general, the positions of the peaks in the conduction plots

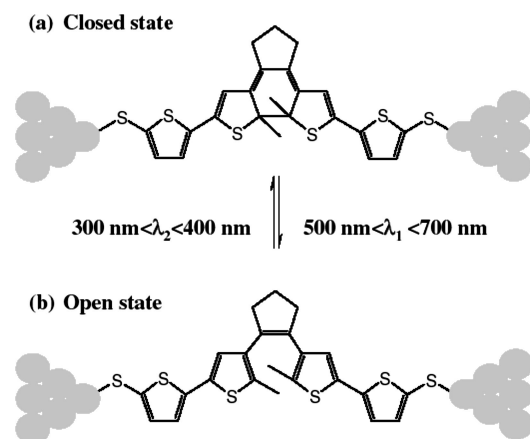


Figure 6. Schematics showing the ideal switching mechanism of the thienylthiophene molecule. Using light of different wavelengths, the molecule can be switched from a less conjugated isomer (open) to a more conjugated isomer (closed) and back. Light of higher energy (with wavelengths between 300 and 400 nm) is needed to transform the molecule from the open state to the closed state, while light of lower energy (with wavelengths between 500 and 700 nm) is needed to switch the molecule from the closed state to the open state. While this transformation can be completed in solution without any problems, the constrained geometry and electronic effects from the electrodes complicate the process in the setup shown with the electrodes. (Reprinted with permission from ref 38b. Copyright 2005 American Chemical Society).

will be a strong function of the exact details and the energetics of the metal–molecule contacts.

Chronologically, the next experiment using MBJs to study molecular conductance³⁷ demonstrated optoelectronic switching of photochromic molecules (Figure 6). Dithienylcyclopentenes have been demonstrated to switch between a fully conjugated (“closed”) isomer to a less conjugated (“open”) isomer upon illumination with different wavelength light sources, both in solution and in the solid state.³⁸ To follow the process, UV–vis spectroscopy was used in solution, and conductance measurements were done in the solid state. The conductivity decreased by 3 orders of magnitude once the molecule was switched from the conjugated (“closed”) state to the unconjugated (“open”) state. Once the molecule was placed across the break junction they were able to successfully switch the molecule from the fully conjugated state to the open state with switching times varying from 20 s to 9 min. The reverse process (i.e., starting with the unconjugated “open” state and switching to the conjugated “closed” state) however could not be achieved. The authors attributed this to quenching of the excited-state by the metal electrodes. They reinforced this argument by performing optical experiments using gold colloids. When the molecules were in solution, they could readily carry out both transitions. However, once the monothiol version of the molecule was attached to a gold colloid, the transformation from the open form to the conjugated form could not be observed, whereas the “closing” process was successfully demonstrated. This, again, reflects the importance and effects of the molecule–metal contact.

The next major improvement to the triple beam MBJs came with a report in 2005 from Champagne et al.³⁹ where a gate electrode was incorporated into the setup to be able to achieve electrostatic control in addition to the control over the coupling (Figure 3). In this study, they were able to place a single fullerene (C_{60}) between the metal contacts and study its transport properties. The electrostatic control provides an

additional “knob” on the electronic levels of the molecules and their alignment (or lack thereof) with the metal’s Fermi level. Using the gate, as well as the mechanical control, they studied the Coulomb blockade as a function of the strength of the coupling to the electrodes and found that the degeneracy point in the Coulomb blockade measurements could be changed through the coupling of the fullerene to the electrodes. A more recent study by the same group⁴⁰ explored the Kondo effect (see Kouwenhoven et al.⁴¹ for further reading) as a function of the electrode coupling. They also elaborated on the distortions of the fullerene molecule as a function of the electrode distance as evidenced by changes in the lowest energy intracage vibrational mode of the molecules.

3.1.2. Break Junctions Based on STM

Break junctions can also be made quickly using a gold STM tip and a gold substrate. The gold tip is first pushed into contact with the substrate causing it to fuse and in the process make a wire. As the tip is subsequently pulled away and the current is measured, the metallic wire that was formed between the tip and the surface gets thinner and thinner, and the measured conductivity decreases in a discrete manner as integer multiples of the quantum of conductance. Eventually the single chain of gold atoms breaks and the conductivity drops to zero unless there are molecules to bridge the gap formed. If there are molecules in the medium in which the breaking process is taking place, they can bridge the gap formed. This technique provides the opportunity of quickly forming over 1000 junctions, and getting good statistics. A histogram, plotted as the number of occurrences vs conductance, has strong peaks around multiples of the quantum of conductance. More peaks will be observed in the region of the histogram between 0 and 1 quantum of conductance. The first examples of this method were reported by Xu et al.⁴² where they applied the technique to two different sets of molecules (Figure 7). First, they used different chain-length alkanedithiols in which the tunneling was in close agreement with earlier reports using AFM techniques. Second, they used 4,4′-bipyridine, which can also coordinate to the gold electrodes through the nitrogens’ lone pairs.

After the initial report, the Tao group, as well as others, used similar methods to measure conductance of single molecules of various chemical compositions.⁴³ In all cases, the data exhibited distinct peaks at integer multiples of the first peak observed in the conductance plots. The β value (defined through the Simmons model that was described in the theoretical overview section and that represents a measure of how fast the tunneling rate decays as a function of distance) could be measured by doing the experiment with a series of molecules of the same chemical composition but different lengths. For example, β is around 1 per $-CH_2-$ in an alkane chain (0.84 \AA^{-1}), 0.87 \AA^{-1} in a peptide chain, and 0.22 \AA^{-1} in a carotenoid chain.⁴³ This approach is very useful, not only because it allows for single molecule measurements, but also because it allows a convenient way of measuring many junctions and distinguishing the statistically significant portion of the data. More recently also by the Tao group⁴⁴ two separate types of conductance quanta were observed when alkanedithiols were measured. The conductances of both sets were also shown to be temperature independent, and the force needed to stretch either type of junction was measured to be the same. Owing to these

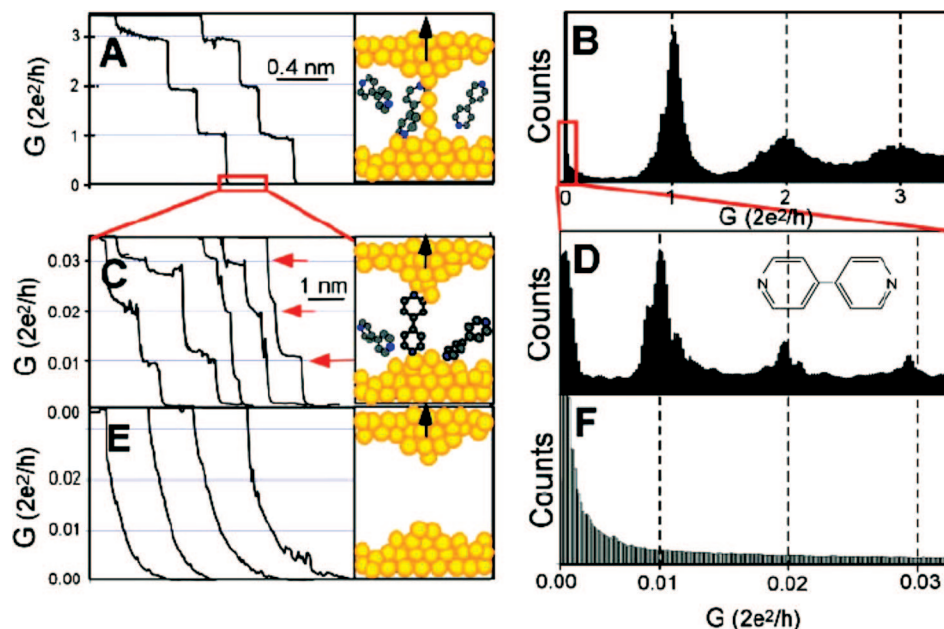


Figure 7. Conductance data for 4--4'-bipyridine (A–D) using the STM-based break junction setup of the Tao group. A and B represent, respectively, the conductance vs distance curves and the histograms collected in the range where metallic filaments dominate the conductance, where C and D show the same plots in the range where molecular conductance is observed. Notice the very large number of repetitions to get useful statistics. E and F represent the conductance vs distance curves and the histogram collected in a control experiment without any bipyridine molecules. Notice the lack of any discrete steps over the relevant range of fractions of the conductance quanta ($2e^2/h$). (Reprinted with permission from *Science* (<http://www.aaas.org>), ref 42. Copyright 2003 American Association for the Advancement of Science).

observations, the differences were ascribed to differences in the molecule electrode contact geometry.

Nishikawa et al.⁴⁵ have extended the STM-based break junction method work on alkanethiols to an ultra high vacuum setup. Their work was able to differentiate between different configurations of the chains being *trans* vs *gauche*. The conductance of the *trans*-rich isomers is measured to be higher than the *gauche*-rich conformations suggesting better electronic coupling.

In a recent review, Ratner and Lindsay⁴⁶ compared a number of experimental results out of the STM-based break junction method to theoretical results using the NEGF-DFT type formalism. Under some reasonable assumptions (i.e., (1) the electronic structure at zero bias does not change at higher biases, (2) the voltage drop is symmetric at the two electrodes, and (3) a metallic slab can be used for the geometry) they calculated the expected conductance. The agreement in most cases is remarkable among a series of alkanes, carotenoids, and polyaniline with the observed and the calculated conductances being of the same order of magnitude (see Table 1). Keeping in mind the historical 5 orders of magnitude discrepancy,⁴⁷ the progress is significant.

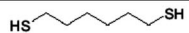

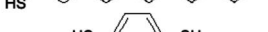
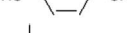
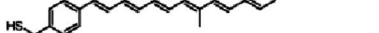
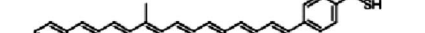
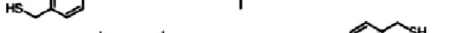

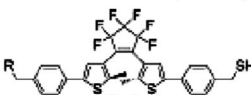
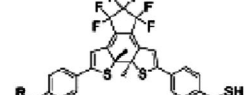
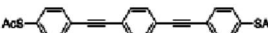
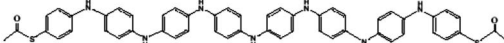
A similar setup has been used by Venkataraman et al.⁴⁸ It is interesting to note that the results of Venkataraman et al. and Tao et al. do not confirm each other. In the work by Venkataraman et al., they were not able to observe any peaks in the conductance histograms when using alkanedithiols. Furthermore, they have not been able to observe more than a single conductance peak for benzene derivatives. Their initial report dealt with the use of different anchoring groups to the metallic surfaces. The conductance histograms showed peaks spread over 2 orders of magnitude for thiol and isonitrile groups (Tao's group uses thiol groups). The amino group, used as an anchor, however, has resulted in the sharpest conductance peaks in the histograms. They have investigated a number of different chain length alkanediamines and found the same β value as Tao did for thiols

(i.e., 1 per $-\text{CH}_2-$). The total conductance, however, was different and would be expected to be different between the amino groups and the thiol groups. In a subsequent report, they studied the effect of twist angle between two phenyl rings and the number of coplanar phenyl rings, on the overall conductance using amino groups as contacts.⁴⁹ The intuitive exponential decrease of conductance with the number of phenyl rings was confirmed. Increased twist angles also decreased the overall conductance with a $\cos^2 \theta$ functional dependence. This indicates, as would be anticipated, that conductance is strongly correlated with the degree of conjugation which also follows a $\cos^2 \theta$ dependence (Figure 8). Next, they varied the chemical substituents on the benzene ring to study the effects of the electronic energy levels on the transport.⁵⁰ By systematically varying the substituents, the ionization potentials of the molecules were changed. The conductance and the calculated tunnel coupling (based on the theory developed by McConnell⁵¹) were found to be inversely dependent on the ionization potential. Moreover, the conductance and the tunnel coupling behaved in a qualitatively similar fashion as a function of the ionization potential. This finding suggested that the conduction arose from hole tunneling through the HOMO levels of the molecules. This is consistent with the fact that most organic conductors are hole conductors: a fact that can simply be explained by comparing the work functions of most electrode materials and the frontier orbital energies of most organic molecules.

The difference between the results of Tao and Venkataraman has been attributed to differences in the selection of the data. The Tao group reports that they select those data sets with a molecule trapped. The Venkataraman work, on the other hand, reportedly proceeds without any prior selection of the data.

The STM-based break junction method can also be extended to include a counter electrode and a reference electrode akin to scanning electrochemical microscopy

Table 1. Comparison of Theoretical and Experimental Values for Conduction Across Different Classes of Molecules^a

	Molecule	G (measured) [nS]	G (theoretical) [nS]	Ratio
1		95 ± 6	185	0.51
2		19.6 ± 2	25	0.78
3		1.6 ± 0.1	3.4	0.47
4		833 ± 90	47 000	0.02
5		2.6 ± 0.05	7.9	0.33
6		0.96 ± 0.07	2.6	0.36
7		0.28 ± 0.02	0.88	0.31
8		0.11 ± 0.07	0.3	0.36
9		1.9 ± 3	0.8	2.4
10		250 ± 50	143	1.74
11		-13	190	0.07
12		0.32 ± 0.03	0.043	7.4

^a All experimental data are from the STM-based break junction measurements of Xu and Tao, and the theoretical calculations were performed with the DFT methodology of Tomfohr and Sankey. Reproduced with permission from ref 46. Copyright 2007 Wiley-VCH Verlag GmbH & Co. KGaA.

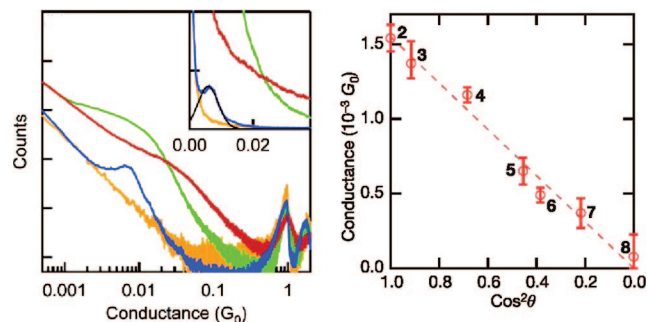


Figure 8. Conductance histograms obtained using an STM-based break junction method by the Venkataraman group. In contrast with the Tao group measurements, there is only one peak corresponding to the molecules. (Left) Dependence of the conductance histograms of modified butanes on the anchoring chemical group. Amines (blue), thiols (red), and isonitriles (green) are explored and compared to a control (yellow) experiment. (Reprinted with permission from ref 48. Copyright 2006 American Chemical Society.) (Right) Modified biphenylene molecules with varying twist angles between the phenyl rings are studied with amino anchoring groups. The effect of the twist angle between two phenylene rings on the conductance is studied (Reprinted with permission from ref 50. Copyright 2007 American Chemical Society).

(SECM). This kind of an approach enables the modulation of the electronic energy levels of the molecule in question through modulations in the potential of the solution relative to the tip and the substrate. This type of solution gating through an electrolyte is much more effective than the conventional solid state gates because the ratios of the capacitances are much more favorable (this is because the potential of an electrolyte solution can be very effectively controlled using a high contact area counter (gate) electrode compared to the contact area of the source and drain). The

pioneering work in this area was done by Tao,⁵² who described the use of the electrochemical potential to amplify or suppress the STM resolution and contrast between an iron containing porphyrin vs a free-base one. When the electrochemical potential is adjusted to the redox potential of the iron porphyrin, the iron center appears higher on the STM image since the tunneling current can be sustained over larger distances when the redox process is added to the base tunneling. When the electrochemical potential is outside the redox peak, there is no contrast because the molecules do not have appreciably different dielectric constants (Figure 9).

The Lindsay group⁵³ has studied a number of aniline oligomers using the above-mentioned STM-based break junction technique under electrochemical potential control. Using this technique they have been able to switch the oligoanilines from the neutral, insulating form, to the oxidized, conducting form, and study the molecular conductance in both cases. It is important to note that assuming tunneling transport leads to a β of 0.08 \AA^{-1} and thus a tunneling gap of 5 mV, which is inconsistent with the very low room temperature conductivity of these materials. Therefore, they suggest that the conductance through oligoanilines is through an activated hopping-type mechanism instead of via direct tunneling (shown in Figure 10).

3.1.3. Electromigrated Break Junctions

Starting from a lithographically defined wire of nanoscale dimensions (typically $<100 \text{ nm} \times 30 \text{ nm}$ in cross section) one can prepare a small gap by applying large biases across. Generally, breaking is not thermal and is termed “electromigration”. Electromigration has been known and studied as

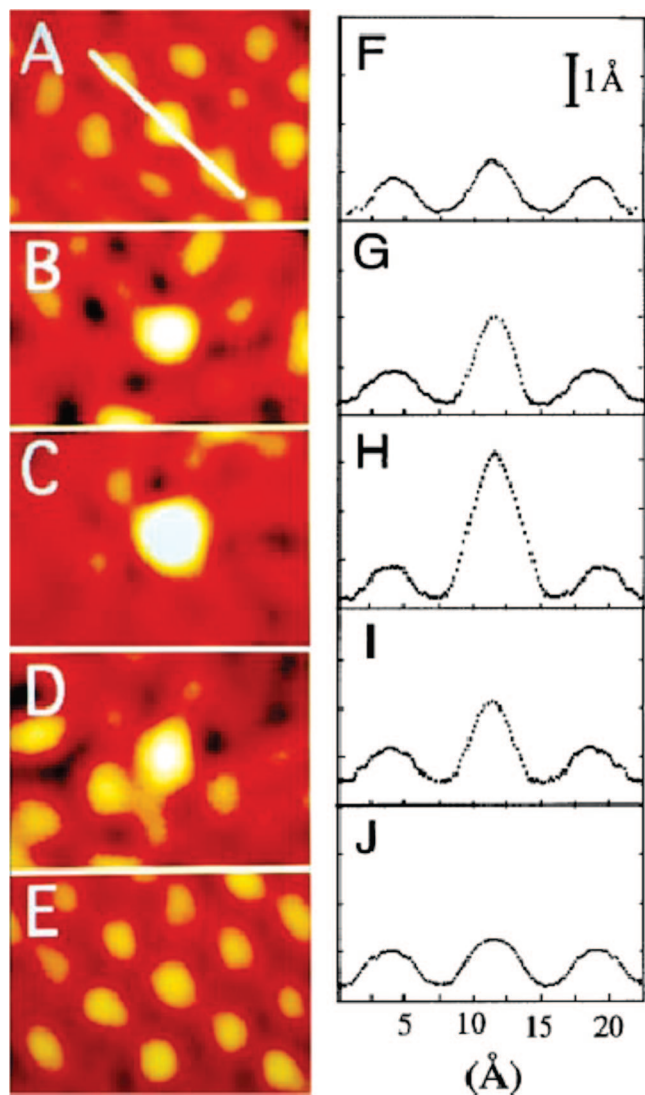


Figure 9. Electrochemical STM images of an iron porphyrin surrounded by free-base porphyrins imaged at different electrochemical potentials ((A) -0.15 V, (B) -0.30 V, (C) -0.42 V, (D) -0.55 V and (E) -0.65 V, with corresponding line traces (F–J)). Notice the change in contrast when the electrochemical potential is outside the window where the iron porphyrin is redox active. The redox conduction at the intermediate potentials enhances the STM signal on the iron porphyrin. (Reprinted with permission from ref 52. Copyright 1996 by the American Physical Society).

one of the major failure modes in electronic circuits.⁵⁴ When the breaking is properly controlled, one can consistently achieve gaps that are ~ 1 nm: the gap size needed to be able to wire up individual molecules.

The initial work using this technique was reported by Hongkun Park et al.⁵⁵ in 1999. Using e-beam lithography and shadow evaporation, they prepared gold electrodes that were 10 nm thick and ~ 150 nm wide at the smallest region. The rest of the contacts to the bonding pads are thicker and wider to be able to keep the largest resistance confined to the region where the break is expected to occur. When a voltage was applied across the wire through a series resistor to limit the current, a sudden increase in the total resistance was observed due to the break forming. The gap size can be estimated using the tunnel resistance right after breaking, or through scanning electron microscopy. The gaps are estimated to be ~ 1 nm using either technique. To deposit the nanocrystals (or molecules), two different approaches can

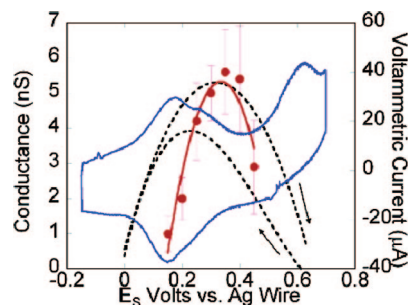


Figure 10. Measured conductance (red dots) and the electrochemical response (blue line) for an aniline oligomer in an STM-based break junction setup embedded in an electrochemical cell. The electrochemical potential control allows for modulating the conductance of the oligoaniline molecules where the state between 0.2 V and 0.6 V vs Ag wire is much more conductive than the states outside of the window. The black dashed line represents a conductance trace of a bulk polyaniline that is converted to the potential scale here and the maximum is scaled to fit the maximum. (Reprinted with permission from ref 53. Copyright 2005 American Chemical Society).

be taken. One can either deposit the nanocrystals and then form the break, or break first and then assemble the nanocrystals. Provided the nanocrystals can survive the breaking process, it is more advantageous to break after deposition for three reasons: (1) the setup does not need to be warmed up between breaking and measurement, (2) the electric field formed during the breaking can assist in trapping the nanocrystals in the gap, and (3) the crystal or molecule “sees” a fresh (and ostensibly clean) gold surface.

After the initial demonstration with nanocrystals, there have been a number of different reports focusing on different properties studied at the single molecule level using this methodology. The initial report on single molecule conductance using electromigrated break junctions by Park et al.⁵⁶ explained conductance through a C_{60} molecule at 1.5 K. Studying the conduction in the Coulomb blockade regime,⁵⁷ information can be obtained not only about the conduction, but also about the coupling of vibrations to the conduction (Coulomb blockade refers to the effect where the Coulomb energy of adding more than one electron to a given island is more than the thermal energy. This dictates that only one electron can be transported through the island at any one time at low biases. Further information can be found in Kouwenhoven et al.⁴³). Because the vibrational energy is higher than the thermal energy available, it can only be excited through the applied potential. Therefore, the vibrational scattering is only effective after the bias across the molecule reaches a certain level which corresponds to the energy of the vibration being studied. The particular mode that was observed was the “bouncing” of the molecule on the electrode surface. To further study vibrations and their coupling to electron transport, Pasupathy et al.⁵⁸ studied a C_{140} in the same geometry. C_{140} is made of two C_{70} molecules tied back-to-back similar to a dumbbell. The major vibrational mode is the stretching of the two C_{70} portions, and the energy associated with it is ~ 11 meV. The study found that, in all devices that were made, the line at 11 meV was always prominent indicating that this mode is highly coupled to the transport.

The Kondo effect was also a major topic of research that made extensive use of electromigrated break junctions. In short, the Kondo effect refers to a second order quantum mechanical process where a spin impurity (e.g., a cobalt atom

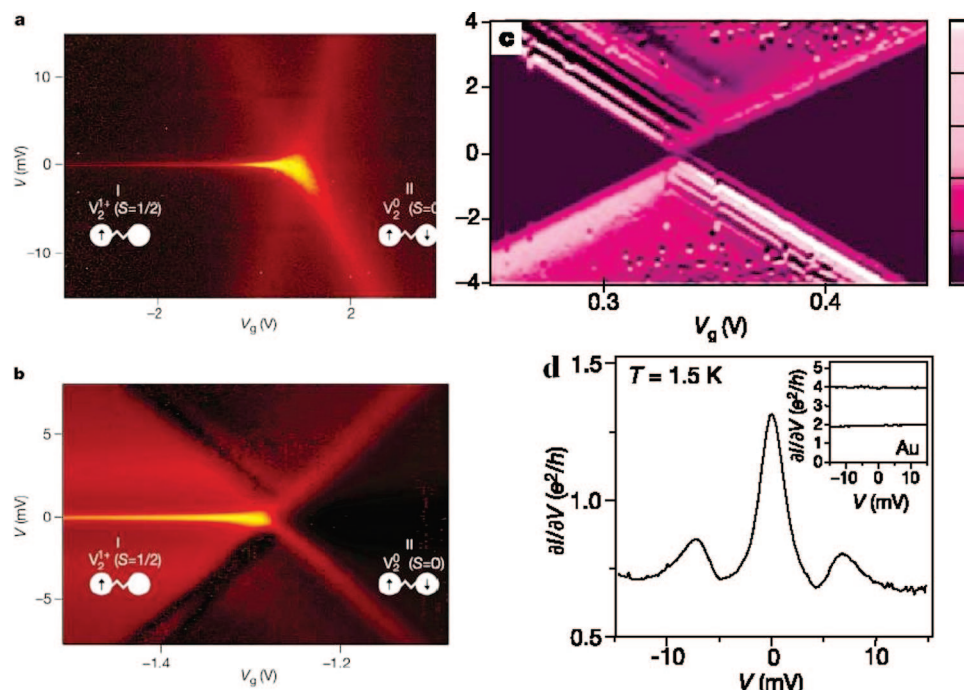


Figure 11. Break junction measurements of transition metal based coordination complexes exhibiting Coulomb blockade and Kondo effect. (a,b) Two separate devices made using a divanadium complex exhibiting both Coulomb blockade and Kondo effect. Notice that the zero bias conductance peak (characteristic of the Kondo effect) only appears when there is an unpaired spin in the molecule. (Reprinted with permission from *Nature* (<http://www.nature.com>), ref 60. Copyright 2002 Nature Publishing Group.) (c) Device exhibiting Coulomb blockade for a bis-terpyridine complex of cobalt with long spacers from the electrode which decrease the coupling between the electrode and the cobalt center. (d) Device exhibiting Kondo effect where alkane spacers were not used thus enhancing the coupling between the electrode and the cobalt center. (Reprinted with permission from *Nature* (<http://www.nature.com>), ref 59. Copyright 2002 Nature Publishing Group).

in bulk copper) decreases the overall conductance by increasing the scattering. For transport across a single molecule where the molecule itself serves as the spin impurity and there is no other conduction channel than the molecule, the Kondo resonance actually enhances the zero bias conduction because it provides another transport mechanism across the dot. In order to observe the Kondo effect in molecular transport experiments, the major requirement is a high degree of coupling between the metallic leads and the spin impurity (note that for Coulomb blockade behavior, a low degree of electrode coupling is required). Two excellent examples, reported back-to-back in 2002 in *Nature*, used organometallic complexes. Park et al.⁵⁹ reported on terpyridyl cobalt complexes where they could tune the coupling of the electrode to the Co center using different alkyl chains and switch the system from one that displayed the Kondo effect to one that displayed Coulomb blockade. In the other report, Liang et al.⁶⁰ employed a system where the coupling was suitable for both the Kondo effect and Coulomb blockade to be present. At some gate electrode bias the molecule has an unpaired spin displaying Kondo effect, and at some other gate bias, the molecule is completely diamagnetic so that only Coulomb blockade behavior was observed (Figure 11). A more recent report⁶¹ on the Kondo effect using break junctions employs a more controlled breaking process whereby the breaking potential is controlled to keep the breaking rate (defined as $(1/R)(\partial R/\partial t)$) constant. Reportedly, the Kondo effect has been observed in $\sim 30\%$ of the devices without any molecules present. The interpretation of the observation is through the leftover gold grains after the breaking process.

3.2. Sandwich Junctions

The junctions referred to in this section are built by depositing (permanently) an electrode on top of a monolayer. The most important experimental variable that has to be investigated is the method of the deposition of the top layer, and the resulting changes to the monolayer due to the specific process employed. We will review a number of methods ranging from e-beam evaporation to electroless deposition followed by electrodeposition, and give examples of each method from the literature.

3.2.1. Evaporation of Metals

Deposition of metals from the vapor phase is a very common technique in semiconductor processing. The metal is heated up until it evaporates and the metal atoms in the vapor phase condense on the desired substrate resulting in a conformal metallic layer. Even though the applicability of this kind of method is suspect when organic monolayers are concerned, there are a number of different reports in the literature reporting devices with this type of top contact. Here we will concentrate on mainly two particular groups: The group at HP Research & Development led by Stan Williams and the collaborative efforts between Mark Reed at Yale and James Tour at Rice. Both groups rely on an evaporated top contact on top of a monolayer of organic molecules using two very different geometries.

Because of the very harsh conditions under which the evaporation process takes place, the stability of the underlying monolayer can be compromised. There have been studies of buried monolayers, trying to assess the effects of the deposition of the top metal layer. In one particular example,

using reflection IR spectroscopy through a thin layer of titanium deposited via the evaporation method,⁶² they found that for an alkanethiol monolayer, the metal reacts with the monolayer resulting in some damage to the top few carbon atoms of each molecule.

The work by the HP group and their collaborators is based on a crossbar geometry where the bottom electrode is either a platinum metal layer, or a titanium oxide layer. Both devices exhibit hysteretic current voltage characteristics, but they are interpreted very differently due to distinct characteristic differences.

The devices with the Pt electrode as the bottom contact have been employed extensively with a number of different molecules.⁶³ The common characteristic in all of these devices is a symmetric hysteretic current voltage profile. This indicates that the physical effect causing the hysteresis is not molecule specific. Additional scanning probe work performed in collaboration with the Bockrath group at CalTech indicated, unequivocally, that specific conduction channels were formed and destroyed through the voltage sweeps. The nature of the conduction channel is still a subject of discussion; however, the current explanation is the formation and dissolution of metallic filaments across the junction.

The devices with the oxide bottom layer, on the other hand, are interpreted to have a different mechanism of operation for two distinct reasons: (1) an asymmetric hysteresis response and (2) a time-dependent current compared to the time-independent current in the devices with metallic electrodes. The behavior is ascribed to a localized charge trap that lowers the tunneling barrier once filled. The barrier empties out once a sufficiently positive potential is applied and subsequently refills once a negative potential is applied again.⁶⁴

The devices that were made by Reed and co-workers in the beginning of this decade relied heavily on the modified phenylene ethynylene oligomers synthesized by the Tour group at Rice. The device architecture is based on a suspended silicon nitride membrane⁶⁵ where a hole smaller than 100 nm in diameter is formed through the membrane and is subsequently metallized from both ends with the molecules deposited in the middle section thus forming a sandwich structure (Figure 12). Temperature-dependent negative differential resistance (NDR) was observed using the modified phenylene ethylenes. The reported peak to valley ratio was 1030:1 at 60 K (Figure 13). The reports also suggest that the NDR effect is not present when alkanethiols are used instead of the phenylene ethynylene oligomers. The interpretation is that the change in the redox state of the molecule is the actual cause of the effect. The interpretation is highly suspect however, since later measurements have indicated^{66,67} that the NDR effect is not an intrinsic property of the molecules.

3.2.2. Electroless Deposition Followed by Electrodeposition

A milder method of making the top contact is through electroless deposition of a seed layer followed by electrodeposition. No hot metal atoms are involved in the process and the deposition is all performed in solution. This technique was demonstrated by Cai et al.⁶⁸ in 2004 making use of track etched membranes as templates.

The manufacturing process involves electrodeposition of the bottom metallic electrode (generally gold, but palladium

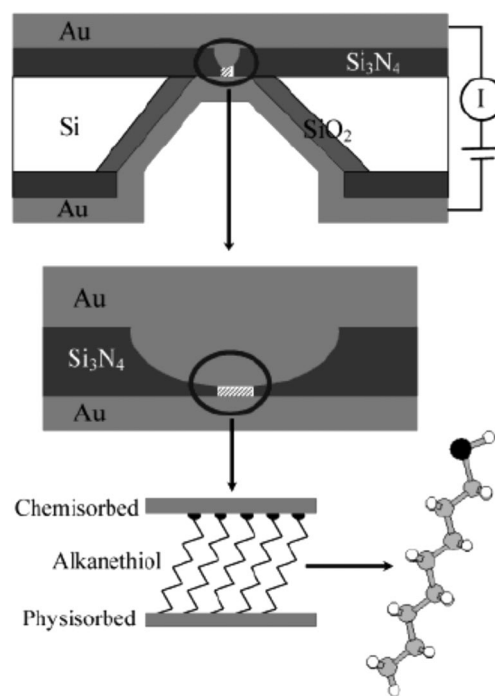


Figure 12. Device schematics used in the “nanopore” measurements. Any self-assembled monolayer can be employed instead of the alkanethiol monolayer depicted here. Note that the bottom “physisorbed” contact is achieved through vapor phase metallization, leaving the integrity of the organic molecules suspect. (Reprinted with permission from ref 65b. Copyright 2004 American Chemical Society).

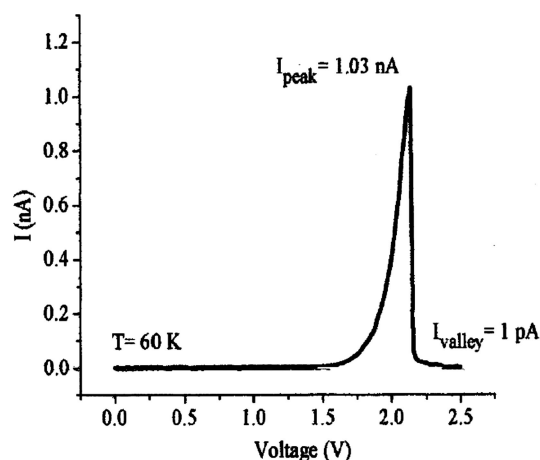


Figure 13. The NDR exhibited by sandwich structures using substituted oligophenyleneethynylene molecules. The experimental setup is depicted in Figure 12. Notice the 1030:1 peak to valley ratio at 60 K. (Reprinted with permission from ref 65a. Copyright 2000, American Institute of Physics).

and silver were also used), followed by potential assisted formation of the monolayer, forming a seed layer on top of the molecular layer from a solution (a process known as electroless deposition), and finally electrodepositing the top electrode on the seed layer deposited out of solution. Once the process is completed, the track etched membranes can be dissolved away, leaving isolated nanowires that have the molecules trapped in the middle. The nanowires are then aligned between two electrodes and the electrical characterization is subsequently performed. In general, current voltage characteristics observed had no unexpected hysteretic loops nor any NDR. They were mostly exponentially dependent tunneling current curves. Three molecules that were studied

were an alkanethiol, an oligophenyleneethynylene (OPE), and an oligophenylenevinylene (OPV).^{69,70} The tunneling currents were much smaller for the alkanethiol when compared to the more conjugated molecules. When the conjugated OPE and OPV were compared with each other, devices made with OPV were found to be more conducting by a factor of more than 5. This was interpreted as being due to a smaller HOMO–LUMO gap due to the increased conjugation through the increased planarity. Furthermore, the study addressed the effect of the contacts on the overall conduction. When palladium rather than gold is used, the conductance measured across the devices made using OPE increased by a factor of 15.

3.2.3. A Liquid Metal Brought into Contact

Historically, mercury drop electrodes have been used by electrochemists mostly due to the ease of obtaining a clean, defect free, metallic surface. For purposes of measuring conductance across assemblies on electrode surfaces, mercury provides a soft (liquid) top electrode in addition to the advantages listed above. Mercury enables researchers to mechanically bring a metallic electrode that can conform to the bottom surface in contact with a molecular assembly. This provides the opportunity of using metallic electrodes for the second contact without the use of any further chemical treatment (electroless deposition) or any hot metal atoms (evaporation).

Even though mercury has historically been very popular and useful, its toxicity limits its utility and other liquid metal surfaces have been explored. A eutectic mixture of gallium and indium is liquid at room temperature and has also been employed in some measurements. In what follows we will focus on mercury, keeping in mind that any liquid metal can be employed for similar measurements.

Experiments using mercury can be divided into two distinct classes: (1) interfaces between two mercury drops and (2) interfaces between mercury and a solid electrode.

3.2.3.1. Mercury–Mercury Junctions. Work done using mercury–mercury junctions has focused on studying electron transport through alkanethiols.⁷¹ Placing two hanging mercury drop electrodes facing each other, the current voltage profile can be monitored as the two mercury surfaces approach each other. Making monolayers on the mercury electrodes allows electron transport through the monolayers to be studied. Even though the stability of these junctions is limited before the two mercury electrodes coalesce and allow only short experimental times, transport could be studied within the 100–1000 s time frame (Figure 14) during which the junctions are stable. Two important conclusions were drawn from these studies: First, the junctions act as perfect parallel plate capacitors, and second, the electron transport does not obey the simple Simmons theory.

When the capacitance of the junction is measured and a plot of inverse capacitance vs the distance between the electrodes is made, a linear dependence is observed. This signifies that the assembly actually acts as an ideal parallel plate capacitor. Furthermore, the dielectric constant obtained from this plot matches previous measurements. Using this dielectric constant, the calculated thicknesses imply no intercalation in the middle, and further imply a perfect bilayer.

Within the Simmons theory, β is predicted to have a square root dependence on the potential difference across the barrier. However, when the data are compiled for a number of

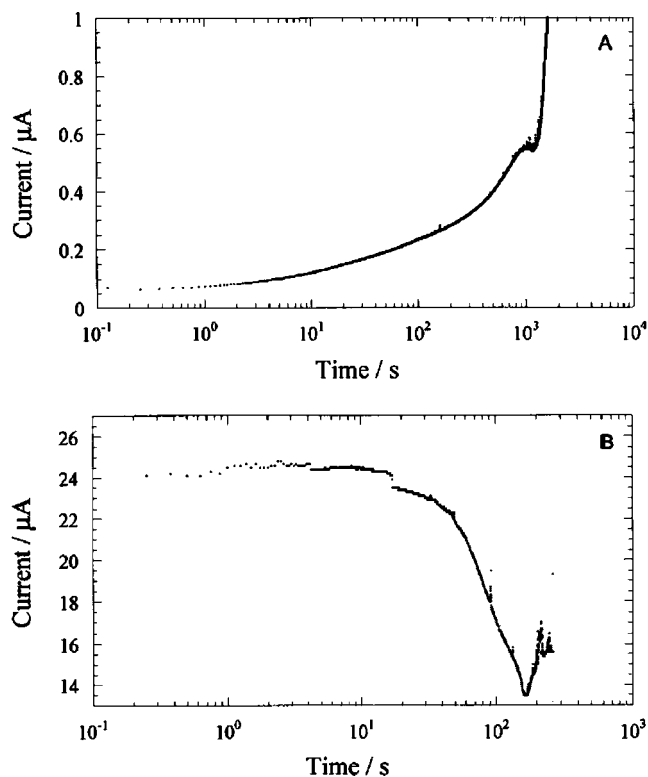


Figure 14. Current vs time traces of two different mercury–mercury junctions immediately after the junctions are formed. Both the mercury drops had self-assembled monolayers of (A) C_{16} . (B) C_{10} alkanethiols formed out of hexadecane solutions. Notice the junctions fail in the 100–1000 s regime. (Reprinted with permission from ref 71b. Copyright 2000 Elsevier).

alkanethiols, only a weak dependence of β on the potential difference was observed. This indicates that the tunneling across alkanethiols cannot be modeled accurately with a square potential barrier.

3.2.3.2. Mercury - Solid Metal Junctions. Bilayers of alkanethiols have also been studied using a mercury drop in contact with a solid metal electrode. The Whitesides group⁷² has studied the electron transport through alkanethiol bilayers using a silver bottom layer and a mercury top contact. They describe, in detail, how the defects on the silver surface affect the conduction across such systems. As illustrated in Figure 15, the density and the nature of the defects in the substrate are very important parameters to keep in mind. When as-deposited silver films are used as the bottom contact, the measured current varies by over 8 orders of magnitude. However, using a substrate prepared by template stripping (obtained by stripping the Ag deposited on a smooth substrate and using the side that was in contact with the smooth substrate), the spread in the current densities measured were brought down to 2 orders of magnitude. The spread in the measured current, when the relatively defect-free substrates were used, was attributed to the effects related to voltage dependent solvent repulsion out of the gap in addition to the defects that are still present on the silver substrate. These junctions were analyzed in detail, and the distribution of the currents was averaged over a very large number of measurements. The calculated β value turned out to be smaller than previously measured. The discrepancy was attributed to the previous experiments being more affected by the surface defects when compared to these.⁷³ Another important observation from the study is the fact that nonbonded junctions did not greatly differ from the bonded ones.

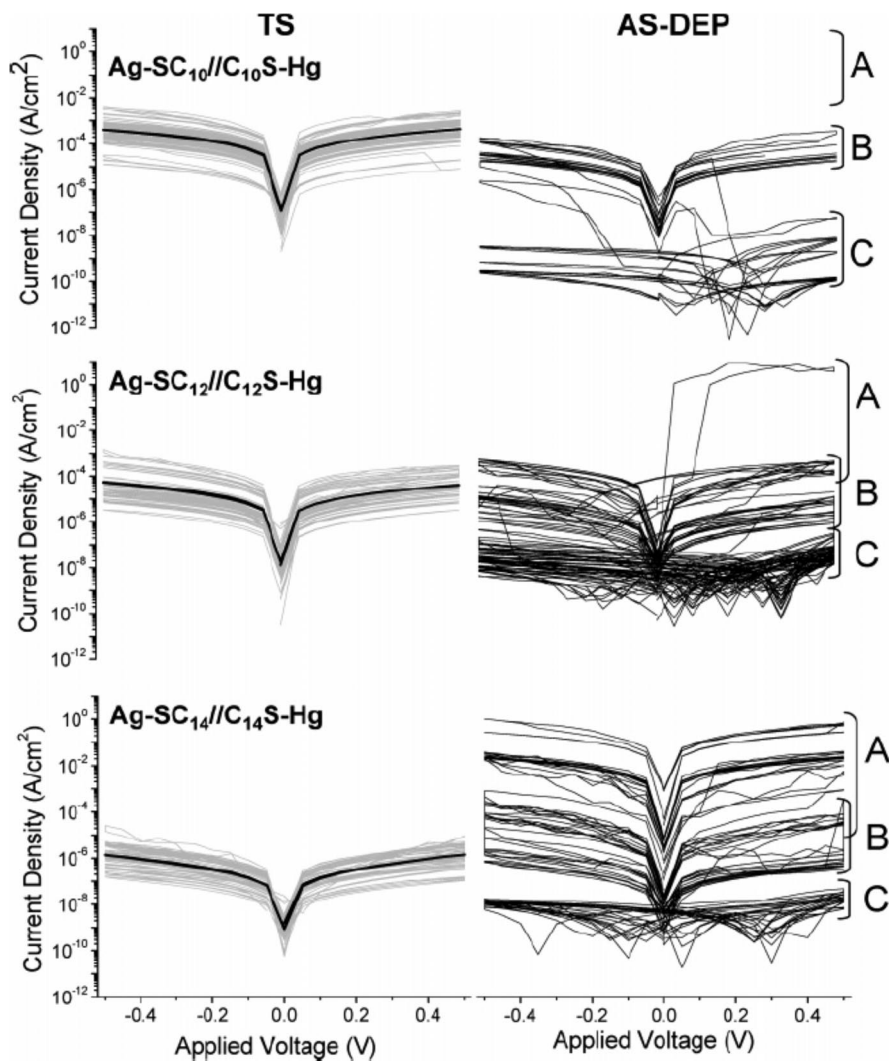


Figure 15. Current density vs potential for three different molecules in the Ag-molecule/molecule-Hg configuration. (Left) The data with a relatively defect free Ag electrode (obtained via the “template stripping” method). (Right) The data with the defect prone “as deposited” Ag electrode. Notice the significance of the use of a defect free substrate in enhancing the reproducibility in the experiments. The spread in the data decreased dramatically when the substrate was smooth. The averages (drawn as heavy black lines) also show a trend of decreasing current density with increasing chain length, consistent with intuition and theoretical predictions. (Reprinted with permission from ref 72. Copyright 2007 American Chemical Society).

In a further study,⁷⁴ asymmetric bilayer junctions were prepared using two different chain length alkane thiols on a gold surface and a mercury top electrode. The resulting current voltage curves were asymmetric, reflecting the asymmetry of the junction. A theoretical method was also developed to interpret and understand the asymmetry in the IV curves.

In another experiment using a mercury electrode and a silicon oxide surface,⁷⁵ a deliberately used redox couple between a thiol mercury bond and a thiolate resulted in stable NDR behavior (Figure 16). The molecule used has a six-membered ring that contains a disulfide bond as shown in the figure. During monolayer formation, the disulfide bond breaks and two mercury sulfur bonds are formed. When an appropriate bias is applied, the mercury sulfide bonds get reduced and two thiolates are formed. Once the thiolates are formed, the conductance drops for two reasons: the contact gets worse, and the negative charge that is formed at the interface creates a barrier. The decreased conductance at higher biases manifests itself as an NDR behavior. The NDR

stability is due to the reversibility of the redox reaction on the mercury electrode.

3.2.4. Mechanical Contact Electrodes

Another area that deserves mention is the area of bringing solid metal electrodes in contact. Two major methods and pioneering groups thereof will be mentioned in this section. The use of conducting probe AFM (CP-AFM) pioneered by the Frisbie group in Minnesota and the use of two cross wires brought together in the presence of a magnetic force pioneered by the Kushmerick group at the Naval Research Laboratory.

The CP-AFM technique is an extension of the standard AFM setup to be able to perform conductance measurements in addition to the force measurements. The major advantage over the scanning tunneling microscope is the ability to control the tip sample separation independently of the conductance, providing a knob on the tip sample contact in addition to the ability to measure conductance of poorly

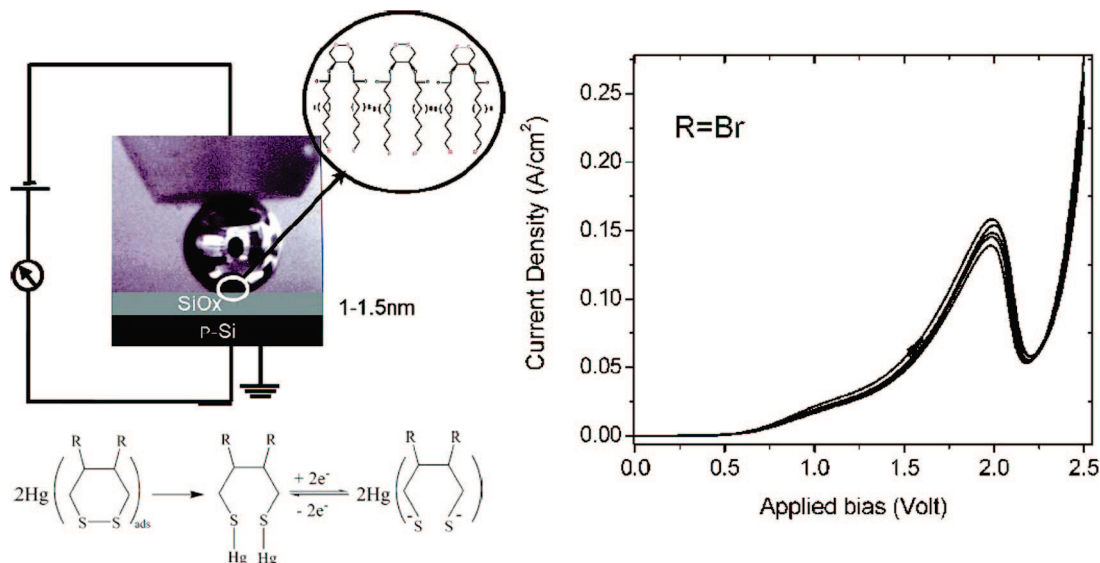


Figure 16. Experimental scheme in which molecules adsorbed on the mercury surface are reduced and oxidized to modulate the conduction across the monolayer. Notice the change in the charge and electronic configuration of the molecules during the voltage sweep. The apparent NDR on the I–V curve is caused by a direct change in the molecular configuration and the electronic states. This well defined NDR scheme is responsible for the very high reproducibility of the experiments. (Reprinted with permission from ref 75. Copyright 2004 American Chemical Society).

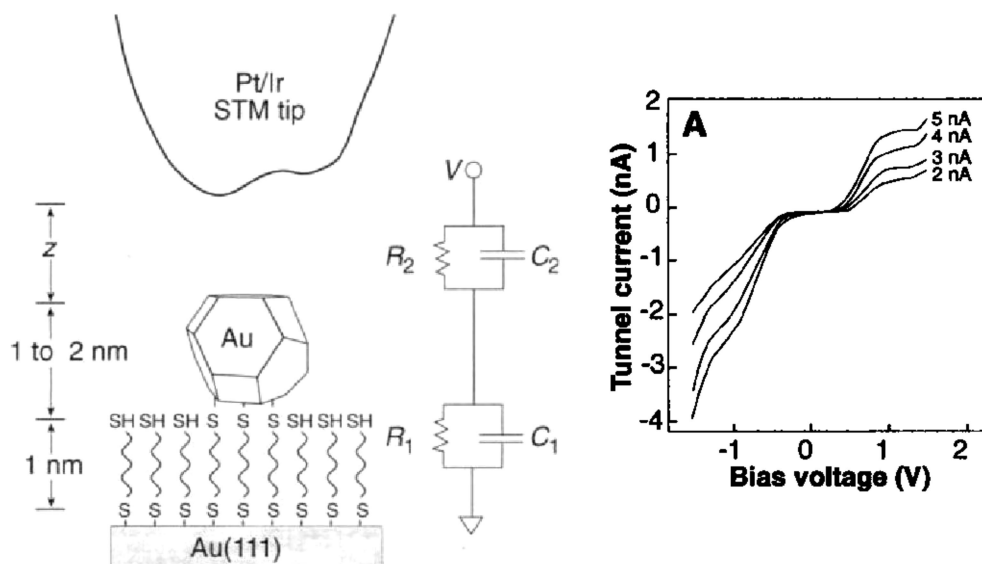


Figure 17. STM experiment with gold nanoparticles on top of an alkanedithiol monolayer and the resulting Coulomb staircase. (Left) The experimental setup where a single crystal surface of Au(111) and a gold nanoparticle were used as the two contacts to the molecular layer. The contact between the STM tip and the Au nanoparticles was facilitated with the feedback loop of the STM circuitry. (Right) The I–V curves with varying setpoints for the tunnel current. Notice the stepwise behavior for different degrees of coupling between the tip and the gold nanoparticle. (Reprinted with permission from *Science* (<http://www.aaas.org>), ref 80. Copyright 1996 American Association for the Advancement of Science).

conducting samples. The use of CP-AFM in characterizing electronic transport across molecular structures was pioneered and developed by the Frisbie group.^{76,77} This technique was successfully employed to study organic crystals⁷⁶ as well as self-assembled monolayers.⁷⁷

The work published by Kushmerick and co-workers^{78,79} has focused on bringing two crosswires together by means of a magnetic force applied to one of the wires. This technique was successfully applied to self-assembled monolayers of a variety of molecules and a couple of important conclusions were drawn. First, because the conductance is found to scale linearly with the area of contact, it is concluded that the molecules do not interact appreciably in a SAM.

Second, when the junction is a rectifying junction (as in Kushmerick et. al), the rectification behavior is very strongly correlated with the strength of the contact between the molecules and the electrode.

3.3. Scanning Tunneling Microscopy

Scanning tunneling microscopy (in addition to the applications mentioned above) has been employed in a number of attempts to study electron transport across molecular assemblies on surfaces. Most of these studies suffered from an uncertainty in the number of molecules contacted by the tip and the nature of that contact. A number of different

methodologies were devised to be able to understand and control the contact between the STM tip and the molecules in question. Here we will review three separate examples, one employing gold clusters, and the other two employing various ways to obtain a low coverage of the molecule in question.

In 1996 Andres et al.⁸⁰ reported on the use of gold clusters on top of a monolayer in an effort to eliminate the complications of the contact between the molecules and the tip itself. The data exhibited a Coulomb staircase due to the large Coulomb energy of adding more than one electron to the cluster. This is because the coupling between the tip and the cluster is nonmetallic. Therefore, the cluster is only capacitively coupled to both the tip and the underlying gold substrate. Using the Coulomb staircase data, the authors were able to extract a resistance value for the monolayers of the molecule to be $18 \pm 12 \text{ M}\Omega$, a value that is within a factor of 4 of the calculated one of $4.5 \pm 0.5 \text{ M}\Omega$ ⁸¹ by some of the same authors in collaboration with others (Figure 17).

An alternative approach was to isolate the molecule in question by making a dilute monolayer of it in the gaps and defects formed by a shorter alkanethiol monolayer.⁸² This work has enabled a thorough investigation of the STM work on oligophenyleneethynylene molecules. The molecules were found to switch between an "ON" and an "OFF" state. The nature of the differences between these states was speculated to be conformational, and not electrostatic through a number of different observations, including, but not limited to the fact that the molecules would switch more often when they are in a less crystalline alkanethiol SAM.

Using another very dilute monolayer technique employing a semiconductor electrode and a metallic tip, the Hersam group at Northwestern reported NDR behavior using two separate molecules of very different nature:⁸³ styrene and TEMPO (2,2,6,6-tetramethyl-1-piperidinyl-oxy). The NDR was explained through the mechanism that was put forward by Datta and co-workers⁸⁴ using a resonant tunneling argument involving the empty orbitals of the molecules.

4. Conclusions

To sum up, both theoretical and experimental methods have been developed in the past two decades to study electron transport through single molecules and assemblies. The theoretical methods are only recently getting to the level of accurately describing molecular assemblies on electrode surfaces. The experience of making exquisitely designed chemically modified electrodes has contributed a great deal to the efforts of measuring conductance through molecules. Experimental methods of making the "second" contact have been developed, even though some are under scrutiny. This remains a very active and fertile area of research that will continue to engage those involved in the basic science and its applications.

5. Acknowledgments

We gratefully acknowledge support by the NSF/NIRT program (Grant CHE-0403806). This work was also supported by Cornell Center for Materials Research (CCMR).

6. References

- (1) Murray, R. W. *Acc. Chem. Res.* **1980**, *13*, 135–141.
- (2) Bakker, E.; Qin, Y. *Anal. Chem.* **2006**, *78*, 3965.
- (3) Chidsey, C. E. D. *Science* **1991**, *251*, 919–922.

- (4) Amatore, C.; Maisonhaute, E.; Schöllhorn, B.; Wadhawan, J. *Chem. Phys. Chem.* **2007**, *8*, 1321.
- (5) Sikes, H. D.; Smalley, J. F.; Dudek, S. P.; Cook, A. R.; Newton, M. D.; Chidsey, C. E. D.; Feldberg, S. W. *Science* **2001**, *291*, 1519–1523.
- (6) Reimers, J. R.; Picconatto, C.; Shashidhar, R. *Molecular Electronics III*; Academy of Sciences: New York, 2003.
- (7) Aviram, A.; Ratner, M. A. *Chem. Phys. Lett.* **1974**, *29*, 277–283.
- (8) Marcus, R. A. *J. Chem. Phys.* **1956**, *24*, 966–978.
- (9) Marcus, R. A. *Pure Appl. Chem.* **1997**, *69* (1), 13–29.
- (10) (a) Mujica, V.; Ratner, M. A. *Chem. Phys.* **2001**, *264*, 365–370. (b) Mujica, V.; Nitzan, A.; Datta, S.; Ratner, M. A.; Kubiak, C. P. *J. Phys. Chem. B* **2003**, *107*, 91–95. (c) Gonzalez, C.; Simon-Manso, Y.; Batteas, J.; Marquez, M.; Ratner, M.; Mujica, V. *J. Phys. Chem. B* **2004**, 18414–18420. (d) Galperin, M.; Nitzan, A.; Ratner, M. A. *Phys. Rev. Lett.* **2006**, *96*, 166803.
- (11) McCreery, R. L. *Chem. Mater.* **2004**, *126* (43), 4477.
- (12) James, D. K.; Tour, J. M. *Chem. Mater.* **2004**, *16* (23), 4423.
- (13) Chen, F.; Hihath, J.; Huang, Z. F.; Li, X. L.; Tao, N. *J. Annu. Rev. Phys. Chem.* **2007**, *58*, 535.
- (14) Nitzan, A.; Ratner, M. A. *Science* **2003**, *300*, 1384.
- (15) Landauer, R. *IBM J.* **1957**, 223.
- (16) Li, C. Z.; Tao, N. *J. Appl. Phys. Lett.* **1998**, *72*, 894.
- (17) Bixon, M.; Jortner, J. *Adv. Chem. Phys.* **1999**, *106*, 35.
- (18) Harold, B.; Ratner, M. A. *J. Chem. Phys.* **2003**, *119*, 11926.
- (19) Troisi, A.; Ratner, M. A. *Phys. Rev. B* **2005**, *72*, 033408.
- (20) Yu, L. H.; Zangmeister, C. D.; Kushmerick, J. G. *Nano Lett* **2006**, *6* (11), 2515–2519.
- (21) Troisi, A.; Beebe, J.; Picraux, L. B.; van Zee, R. D.; Stewart, D. R.; Ratner, M. A.; Kushmerick, J. G. *Proc. Natl. Acad. Sci.* **2007**, *104* (36), 14255–14259.
- (22) Kushmerick, J. G.; Lazorcik, J.; Patterson, C. H.; Shashidhar, R.; Seferos, D. S.; Bazan, G. C. *Nano Lett.* **2004**, *4*, 639.
- (23) Ke, S.-H.; Baranger, H. U.; Yang, W. *J. Chem. Phys.* **2005**, 074704.
- (24) Sai, N.; Zwolak, M.; Vignale, G.; Di Ventra, M. *Phys. Rev. Lett.* **2005**, 186810.
- (25) Toher, C.; Filipetti, A.; Sanvito, S.; Burke, K. *Phys. Rev. Lett.* **2005**, 146402.
- (26) Koentopp, M.; Burke, K.; Evers, F. *Phys. Rev. B* **2006**, 121403.
- (27) Simmons, J. G. *J. Appl. Phys.* **1963**, *34*, 1793–1803.
- (28) Monnell, J. D.; Stapleton, J. J.; Dirk, S. M.; Reinerth, W. A.; Tour, J. M.; Allara, D. L.; Weiss, P. S. *J. Phys. Chem. B* **2005**, *109* (43), 20343–20349.
- (29) Ortiz, D. O.; Seminario, J. M. *J. Chem. Phys.* **2007**, *127*, 111106.
- (30) Jortner, J.; Nitzan, A.; Ratner, M. A. In *Introducing Molecular Electronics*; Springer: Berlin/Heidelberg 2006.
- (31) Nitzan, A. *J. Phys. Chem. A* **2001**, *105*, 2677.
- (32) Moreland, J.; Ekin, J. W. *J. Appl. Phys.* **1985**, *58* (10), 3888–3895.
- (33) Reed, M. A.; Zhou, C.; Muller, C. J.; Burgin, T. P.; Tour, J. M. *Science* **1997**, *278*, 252–253.
- (34) Schneir, J.; Sonnenfeld, R.; Marti, O.; Hansma, P. K.; Demuth, J. E.; Hamers, R. J. *J. Appl. Phys.* **1988**, *63* (3), 717–721.
- (35) Troisi, A.; Ratner, M. A. *Mol. Nanoelectronics* **2003**, 1–18.
- (36) Reichert, J.; Ochs, R.; Beckmann, D.; Weber, H. B.; Mayor, M.; Löhneysen, H. v. *Phys. Rev. Lett.* **2002**, *88*, 176804.
- (37) Dulic, D.; Molen, S. J. v. d.; Kudernac, T.; Jonkman, H. T.; Jong, J. J. D. d.; Bowden, T. N.; Esch, J. v.; Feringa, B. L.; Wees, B. J. v. *Phys. Rev. Lett.* **2003**, *91*, 207402.
- (38) (a) Irie, M. *J. Org. Chem.* **1988**, *53*, 803. (b) Irie, M.; Fukaminato, T.; Sasaki, T.; Tamai, N.; Kawai, T. *Nature* **2002**, *420*, 759.
- (39) Champagne, A. R.; Pasupathy, A. N.; Ralph, D. C. *Nano Lett.* **2005**, *5*, 305–308.
- (40) Parks, J. J.; Champagne, A. R.; Hutchison, G. R.; Flores-Torres, S.; Abruña, H. D.; Ralph, D. C. *Phys. Rev. Lett.* **2007**, *99*, 026601.
- (41) Kouwenhoven, L.; Glazman, L. *Phys. Today* **2001**, 33.
- (42) Xu, B.; Tao, N. *Science* **2003**, *301*, 1221–1223.
- (43) Tao, N. *J. Mater. Chem.* **2005**, *15*, 3260–3263, and the references therein.
- (44) Li, X.; He, J.; Hihath, J.; Xu, B.; Lindsay, S. M.; Tao, N. *J. Am. Chem. Soc.* **2006**, *128*, 2135–2141.
- (45) Nishikawa, A.; Tobita, J.; Kato, Y.; Fujii, S.; Suzuki, M.; Fujihira, M. *Nanotechnology* **2007**, *18*, 424005.
- (46) Lindsay, S. M.; Ratner, M. A. *Adv. Mater.* **2007**, *19*, 23–31.
- (47) Salomon, D.; Cahen, D.; Lindsay, S.; Tomfohr, J.; Engelkes, V. B.; Frisbie, C. D. *Adv. Mater.* **2003**, *15*, 1881.
- (48) Venkataraman, L.; Klare, J. E.; Tam, I. W.; Nuckolls, C.; Hybertsen, M. S.; Steigerwald, M. L. *Nano Lett.* **2006**, *6*, 458–462.
- (49) Venkataraman, L.; Klare, J. E.; Nuckolls, C.; Hybertsen, M. S.; Steigerwald, M. L. *Nature* **2006**, *442*, 904–907.
- (50) Venkataraman, L.; Park, Y. S.; Whalley, A. C.; Nuckolls, C.; Hybertsen, M. S.; Steigerwald, M. L. *Nano Lett.* **2007**, *7*, 502–506.
- (51) McConnell, H. *J. Chem. Phys.* **1961**, *35*, 508–515.
- (52) Tao, N. *Phys. Rev. Lett.* **1996**, *76*, 4066.

- (53) Chen, F.; He, J.; Nuckolls, C.; Roberts, T.; Klare, J.; Lindsay, S. M. *Nano Lett.* **2005**, *5*, 503.
- (54) Ho, P. S.; Kwok, T. *Rep. Prog. Phys.* **1989**, *52*, 301.
- (55) Park, H.; Lim, A. K. L.; Alivisatos, A. P.; Park, J.; McEuen, P. L. *Appl. Phys. Lett.* **1999**, *75*, 301.
- (56) Park, H.; Park, J.; Lim, A. K. L.; Anderson, E. H.; Alivisatos, A. P.; McEuen, P. L. *Nature* **2000**, *407*, 57.
- (57) Kouwenhoven, L.; Schön, G.; Sohn, L. L. *Mesoscopic Electron Transport*; Kluwer: Dordrecht, 1997.
- (58) (a) Park, J.; Pasupathy, A. N.; Goldsmith, J. I.; Soldatov, A. V.; Chang, C.; Yaish, Y.; Sethna, J. P.; Abruña, H. D.; Ralph, D. C.; McEuen, P. L. *Thin Sol. Films* **2003**, *438–439*, 457. (b) Pasupathy, A. N.; Park, J.; Chang, C.; Soldatov, A. V.; Lebedkin, S.; Bialczak, R. C.; Grose, J. E.; Donev, L. A. K.; Sethna, J. P.; Ralph, D. C.; McEuen, P. L. *Nano Lett.* **2005**, *5*, 203.
- (59) Park, J.; Pasupathy, A. N.; Goldsmith, J. I.; Chang, C.; Yaish, Y.; Petta, J. R.; Rinkoski, M.; Sethna, J. P.; Abruña, H. D.; McEuen, P. L.; Ralph, D. C. *Nature* **2002**, *417*, 722.
- (60) Liang, W.; Shores, M. P.; Bockrath, M.; Long, J. R.; Park, H. *Nature* **2002**, *417*, 725.
- (61) Houck, A. A.; Labaziewicz, J.; Chan, E. K.; Folk, J. A.; Chuang, I. L. *Nano Lett.* **2005**, *5*, 1685–1688.
- (62) Donley, C. L.; Blackstock, J. J.; Stickle, W. F.; Stewart, D. R.; Williams, R. S. *Langmuir* **2003**, *23*, 7620.
- (63) (a) Lau, C. N.; Stewart, D. R.; Williams, R. S.; Bockrath, M. *Nano Lett.* **2004**, *4*, 569–572. (b) Lau, C. N.; Stewart, D. R.; Bockrath, M.; Williams, R. S. *Appl. Phys. A: Mater. Sci. Process.* **2005**, *80*, 1373–1378.
- (64) (a) Collier, C. P.; Wong, E. W.; Belohradsky, M.; Raymo, F. M.; Stoddart, J. F.; Kuekes, P. J.; Williams, R. S.; Heath, J. R. *Science*, **1999**, *285*, 391. (b) Richter, C. A.; Stewart, D. R.; Ohlberg, D. A. A.; Williams, R. S. *Appl. Phys. A: Mater. Sci. Process.* **2005**, *80*, 1355–1362.
- (65) (a) Chen, J.; Wang, W.; Reed, M. A.; Rawlett, A. M.; Price, D. W.; Tour, J. M. *Appl. Phys. Lett.* **2000**, *77*, 1224. (b) Lee, T.; Wang, W.; Klemic, J. F.; Zhang, J. J.; Su, J.; Reed, M. A. *J. Phys. Chem. B* **2004**, *108*, 8742–8750.
- (66) Tour, J. M.; Cheng, L.; Nackashi, D. P.; Yao, Y.; Flatt, A. K.; Angelo, S. K.; Mallouk, T. E.; Franzon, P. D. *J. Am. Chem. Soc.* **2003**, *127*, 13279–13283.
- (67) Keane, Z. K.; Cizsek, J. W.; Tour, J. M.; Natelson, D. *Nano Lett.* **2006**, *6*, 1518.
- (68) Cai, L. T.; Skulason, H.; Kushmerick, J. G.; Pollack, S. K.; Naciri, J.; Shashidhar, R.; Allara, D. L.; Mallouk, T. E.; Mayer, T. S. *J. Phys. Chem. B* **2004**, *108*, 2827–2832.
- (69) Kushmerick, J. G.; Holt, D. B.; Pollack, S. K.; Ratner, M. A.; Yang, J. C.; Schull, T. L.; Naciri, J.; Moore, M. H.; Shashidhar, R. *J. Am. Chem. Soc.* **2002**, *124*, 10645–10655.
- (70) Tour, J. M.; Rawlett, A. M.; Kozaki, M.; Yao, Y. X.; Jagessar, R. C.; Dirk, S. M.; Price, D. W.; Reed, M. A. *Chem.-Eur. J.* **2001**, *7*, 5118–5134.
- (71) (a) Slowinski, K.; Fong, H. K. Y.; Majda, M. *J. Am. Chem. Soc.* **1999**, *121*, 7257–7261. (b) Slowinski, K.; Majda, M. *J. Electroanal. Chem.* **2001**, *491*, 139–147.
- (72) Weiss, E. A.; Chiechi, R. C.; Kaufman, G. K.; Kriebel, J. K.; Li, Z.; Duati, M.; Rampi, M. A.; Whitesides, G. M. *J. Am. Chem. Soc.* **2007**, *129*, 4336–4349.
- (73) (a) Sek, S.; Bilewicz, R.; Slowinski, K. *Chem. Commun.* **2004**, 404. (b) York, R. L.; Nguyen, P. T.; Slowinski, K. *J. Am. Chem. Soc.* **2003**, *125*, 5948.
- (74) Galperin, M.; Nitzan, A.; Sek, S.; Majda, M. *J. Electroanal. Chem.* **2000**, *550–551*, 337–350.
- (75) Salomon, A.; Arad-Yelin, R.; Shanzer, A.; Karton, A.; Cahen, D. *J. Am. Chem. Soc.* **2004**, *126*, 11648.
- (76) Kelly, T. W.; Ganstrom, E. L.; Frisbie, C. D. *Adv. Mater.* **1999**, *11*, 261.
- (77) Wold, D. J.; Frisbie, C. D. *J. Am. Chem. Soc.* **2001**, *123*, 5549.
- (78) Kushmerick, J. G.; Naciri, J.; Yang, J. C.; Shashidhar, R. *Nano Lett.* **2003**, *3*, 897.
- (79) Kushmerick, J. G.; Whitaker, C. M.; Pollack, S. K.; Schull, T. L.; Shashidhar, R. *Nanotechnology* **2004**, *15*, S489.
- (80) Andres, R. P.; Bein, T.; Dorogi, M.; Feng, S.; Henderson, J. I.; Kubiak, C. P.; Mahoney, W.; Osifchin, R. G.; Reifenberger, R. *Science* **1996**, *272*, 1323–1325.
- (81) Samanta, M. P.; Tian, W.; Datta, S.; Henderson, J. I.; Kubiak, C. P. *Phys. Rev. B* **1996**, *53*, 7626.
- (82) (a) Dunbar, T. D.; Cygan, M. T.; Bumm, L. A.; McCarty, G. S.; Burgin, T. P.; Reinerth, W. A.; Jones, L.; Jackiw, J. J.; Tour, J. M.; Weiss, P. S.; Allara, D. L. *J. Phys. Chem. B* **2000**, *104*, 4880–4893. (b) Donhauser, Z. J.; Mantoosh, B. A.; Kelly, K. F.; Bumm, L. A.; Monnell, J. D.; Stapleton, J. J.; Price, D. W.; Rawlett, A. M.; Allara, D. L.; Tour, J. M.; Weiss, P. S. *Science* **2001**, *292*, 2303.
- (83) Guisinger, N. P.; Greene, M. E.; Basu, R.; Baluch, A. S.; Hersam, M. C. *Nano Lett.* **2004**, *4*, 55–59.
- (84) Rakshit, T.; Liang, G.-C.; Ghosh, A. W.; Datta, S. *Nano Lett.* **2003**, *4*, 1803.

CR068060W